Photon-Mediated Thermoelectric and Heat Currents through a Resonant Quantum Wire-Cavity System

Nzar Rauf Abdullah [1,2,3,*] **, Rawezh Bakr Marif** [1,†] **and Hunar Omar Rashid** [1,†]

1   Physics Department, College of Science, University of Sulaimani, Sulaymaniyah, Iraq
2   Komar Research Center, Komar University of Science and Technology, Sulaimani, Iraq
3   Science Institute, University of Iceland, Dunhaga 3, IS-107 Reykjavik, Iceland
*   Correspondence: nzar.r.abdullah@gmail.com; Tel.: +964-770-144-3854
†   These authors contributed equally to this work.

Abstract: We theoretically consider a short quantum wire, which on both ends is connected to leads that have different temperatures. The quantum wire is assumed to be coupled to a cavity with a single-photon mode. We calculate the heat and thermoelectric currents in the quantum wire under the effect of the photon field. In the absence of the photon field, a plateau in the thermoelectric current is observed due to the thermal smearing at a high temperature gradient. In the presence of the resonance photon field, when the energy spacing between the lowest states of the quantum wire is approximately equal to the photon energy, a suppression in thermoelectric current and negativity in the heat current are seen due to the dressed electron-photon states. It is also found that the cavity with high photon energy has more influence on the thermoelectric current at a high temperature gradient.

1. Introduction

Efficient energy consumption is one of the most important areas of research in bulk [1,2] and nanoscale materials [3]. Nanoscale devices have a good potential for application in energy harvesting, which makes them of interest to researchers [4]. Especially, thermoelectric transport is one of the most important areas of interest that is actively investigated [5]. Thermoelectric current can be generated by a temperature gradient between two nanoscale materials connected by a tunneling region in which thermoelectric and heat currents can be transferred by phonons [6] or electrons [7].

The thermoelectric efficiency of a material is measured by a dimensionless number known as the figure of merit (ZT), which is a quantity used to characterize the performance of thermoelectric devices [8]. In bulk semiconductor materials, ZT is increased only marginally, from about 0.6 to 1 [9,10]. However, nanomaterials can have a relatively high ZT because of their low dimensionality [9,11]. In addition, nanoscale materials have been used to enhance thermoelectric efficiency in two ways: first, by using them to introduce quantum confinement to improve the power factor; second, the nanostructured materials add many internal interfaces that scatter phonons [12]. Several nanostructured systems have been investigated for these purposes, such as single quantum dots [13,14], double quantum dots [15,16], triple quantum dots [17], and quantum wells [18].

Another interesting phenomena in nanodevices is the Coulomb blockade, which influences the figure of merit in quantum systems [19]. It has been shown that, in the absence of Coulomb interaction, ZT can only be high if a single energy level in the quantum dot is considered; however, with the consideration of the Coulomb interaction, ZT can be high for multilevel energies [19].

The role of spin, including Zeeman spin [20] and spin-orbit coupling such as the Rashba effect [21], in thermal transport has been of interest for investigating thermospin current in non-conventional spintronic devices. It is shown that the Rashba spin-orbit coupling forms Fano-like interference effects, which result in an enhanced thermoelectric response [22]. Tuning the Rashba coefficient, anti-crossings in the energy spectrum have been observed leading to the Aharonov–Casher destructive phase interference in the quantum ring system [23,24]. As a result, maximum spin polarization is found at the points of anti-crossings due to spin accumulation in the system.

The effect of the photon field on both heat [25] and thermoelectric transport [26] has also been demonstrated. The thermoelectric current between two materials, mediated by photon fluctuations, can be enhanced with an intermediate quantum circuit, leading to the device concept of a mesoscopic photon heat transistor [27]. This proposed device may be used to generate a thermal amplifier and modulator in nano-scale systems [28]. In addition, it has been reported that heat can be transferred by a quantized photon when the phonons are frozen out at a very low temperature [29], and the photon field can change both the magnitude and the sign of the electrical voltage induced by the temperature gradient [30], which plays the role of a thermal amplifier.

In this paper, we investigate thermoelectric and heat transport through a quantum wire coupled to two leads that are at different temperatures. In addition, the quantum wire is coupled to a photon cavity with a single photon mode. The aim is to investigate theoretically the thermoelectric transport under the influence of a photon field in the resonance regime.

The paper is divided into the following sections. In Section 2, the theoretical model is elaborated. In Section 3, we show the results. Lastly, some concluding remarks are presented in Section 4.

2. Model

In this section, we demonstrate the theoretical model underpinning the system. We have a quantum wire that is coupled to two semi-infinite leads along the x-axis and is parabolically confined in the y-axis. This system is itself coupled to a photon cavity. The total system, the quantum wire coupled to the cavity and the leads, is shown in Figure 1a. The magenta zigzag arrows demonstrate the photon field inside the cavity (magenta rectangle) coupled to the quantum wire. The temperature of the hot lead (T_h) (red color) is considered to be higher than that of the cold lead (T_c) (blue color). Figure 1b shows the potential representing the quantum wire.
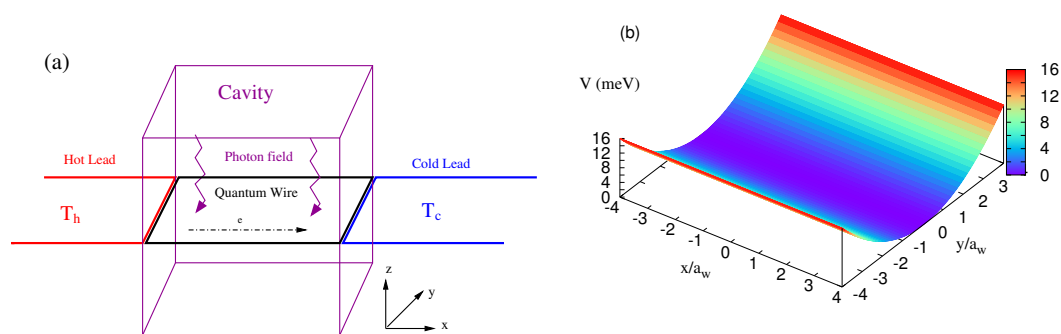
Figure 1. (**a**) Schematic diagram displaying the quantum wire (black) coupled to the leads, where the temperature of the hot lead (left lead) (T_h) (red) is higher than the temperature of the cold lead (right lead) (T_c) (blue). The magenta zigzag displays the photon field in the cavity (magenta rectangle). (**b**) The potential $V_r(\mathbf{r})$ defining the central quantum wire that will be coupled diametrically to the semi-infinite left and right leads in the x-direction. The magnetic field is $B = 0.1$ T, and $\hbar\Omega_0 = 2.0$ meV.

The total system is put under the influence of a perpendicular static magnetic field with a magnitude of $B = 0.1$ T. The electron distribution in the leads is described by the Fermi distribution function:

$$f_{h/c} = \left[1 + \exp\left((E - \mu_{h/c})/(k_B T_{h/c})\right)\right]^{-1}. \tag{1}$$

where $\mu_h(T_h)$ is the chemical potential (temperature) of the hot lead and $\mu_c(T_c)$ is the chemical potential (temperature) of the cold lead. We assume that the temperature of the left lead is higher than that of the right lead, i.e., the left lead is the hot lead.

The Hamiltonian of the coupled electron-photon system is given by:

$$\hat{H}_S = \int d^2r\, \hat{\psi}^\dagger(\mathbf{r}) \left[\frac{1}{2m^*}\left(\frac{\hbar}{i}\nabla + \frac{e}{c}\hat{\mathbf{A}}_B(\mathbf{r})\right) + V_{QW} + eV_g\right]^2 \hat{\psi}(r)$$
$$+ H_Z + H_C + H_\gamma + H_p + H_d. \tag{2}$$

Herein, $\hat{\psi}$ is the electron field operator, and $\hat{\mathbf{A}}_B$ is the magnetic vector potential in which $\mathbf{A}_B(\mathbf{r}) = -By\hat{x}$ defined in the Landau gauge. The photon field is introduced by $\hat{\mathbf{A}}_\gamma(\mathbf{r}) = A(\hat{a} + \hat{a}^\dagger)e$, where A is the amplitude of the photon field given by the electron-photon coupling constant $g_\gamma = eAa_w\Omega_w/c$. The photon can be parallelly polarized ($e = e_x$) or it can be perpendicularly polarized ($e = e_y$) to the electron transport in the quantum wire. The effective electron confinement in the quantum wire is given by $\Omega = \sqrt{\Omega_0^2 + \omega_c^2}$, where Ω_0 is the electron confinement frequency due to the lateral parabolic potential and ω_c is the cyclotron frequency due to the external magnetic field. The quantum wire can be defined by:

$$V_{QW} = \frac{1}{2}m^*\Omega_0^2 y^2 \times \theta\left(\frac{L_x}{2} - |x|\right) \tag{3}$$

with $L_x = 150$ nm the length of the quantum wire and θ the Heaviside step function. We choose parabolic potential in the y-direction because it is a more realistic potential. In actual quantum wires, the confining potential can be approximated by a parabolic potential. Furthermore, V_g indicates the gate voltage that moves the energy states of the quantum wire with respect to the chemical potential of the leads.

In the second line of Equation (2), $H_Z = \pm g^*\mu_B B/2$ is the Zeeman Hamiltonian defining the interaction between the magnetic moment of an electron and the external magnetic field (B), with μ_B the Bohr magneton and $g^* = -0.44$ the effective g-factor for GaAs. H_C is the Coulomb interaction Hamiltonian between the electrons in the quantum wire [31,32]. It should be mentioned that the Coulomb interaction is neglected in the leads. In addition, $H_\gamma = \hbar\omega_\gamma a^\dagger a$ indicates the free photon field where $\hbar\omega_\gamma$ is the photon energy and $a^\dagger(a)$ is the photon creation (annihilation) operator, respectively. The electron–photon and electron–electron interactions are taken into account step-wise through exact diagonalization methods and truncation [25,33]. The last two terms of the second line of Equation (2) are the paramagnetic Hamiltonian:

$$H_p = -\frac{1}{c}\int d^2r\, \mathbf{j}(\mathbf{r}) \cdot \mathbf{A}_\gamma \tag{4}$$

and diamagnetic Hamiltonian:

$$H_d = -\frac{e}{2m^*c^2}\int d^2r\, \rho(\mathbf{r})A_\gamma^2 \tag{5}$$

that describe the electron–photon interactions where ρ and J are the charge and the charge-current densities, respectively [34,35].

To calculate the evolution of the electron in the system, we use a non-Markovian master equation, which describes the time-dependent evolution of the system in non-equilibrium conditions [25,36].

The reduced density operator $\hat{\rho}_S$ that defines the state of the electrons in the quantum wire under the influence of the leads is:

$$\hat{\rho}_S(t) = \text{Tr}_l[\hat{\rho}(t)], \tag{6}$$

where $\hat{\rho}(t)$ is the density matrix of the total system, and the trace is over the Fock space of the leads [37]. l refers to the left (L) or hot (h) lead and the right (R) or cold (c) lead here. The density matrix of the total system before the coupling to the leads is $\hat{\rho}(t_0) = \hat{\rho}_l(t_0)\hat{\rho}_S(t_0)$, where $\hat{\rho}_S(t_0)$ is initial value of the density matrix of the quantum wire and $\hat{\rho}_l(t_0)$ are the density matrix operators of the l lead.

Once the reduced density matrix is known, the physical observables, such as thermoelectric current (I_{TH}), can be calculated. (I_{TH}) is given by:

$$I_{\text{TH}}^{h,c} := \text{Tr}[\hat{\rho}_S^{h,c}(t)\hat{Q}] \tag{7}$$

Herein, $\hat{Q} = e\hat{N}_e$ is the charge operator, and $\hat{N}_e$ is the electron number operator. The thermoelectric current from the left lead (hot lead) into the quantum wire is defined as I_{TH}^h, and the thermoelectric current from it into the right lead (cold lead) is I_{TH}^c.

The heat current (I_H) can be calculated using:

$$\begin{aligned} I_H^{h,c} &:= \text{Tr}\left[\hat{\rho}_S^{h,c}(t)(\hat{H}_S - \mu\hat{N}_e)\right] \\ &= \sum_{ij}\langle i|\hat{\rho}_S^{h,c}|j\rangle(E_i - \mu\hat{N}_e)\delta_{ij}. \end{aligned} \tag{8}$$

Again, the heat current from the left lead (hot lead) into the quantum wire is I_H^h, and the heat current from it into the right lead (cold lead) is I_H^c. In the steady-state condition, the left and right currents are of equal magnitude and opposite direction, and in other cases, a charging or discharging of the central system will take place. Our system approaches the steady-state regime at $t = 220$ ps, in which the left and the right thermoelectric currents are almost equal in magnitude.

3. Results

We present the results of the quantum wire coupled to the photon cavity. The total system, the quantum wire and the leads, was exposed to a weak external magnetic field $B = 0.1$ T, implying the effective magnetic length to be $a_w = 23.8$ nm. The magnetic field lifted the spin degeneracy, Zeeman spin, which otherwise may create numerical difficulties. One more reason to have the low magnetic field here is to avoid circular motion of charge due to the Lorentz force, which in turn may influence the thermoelectric current [37]. The electron confinement energy was assumed to be $\hbar\Omega_0 = 2.0$ meV, and the cyclotron energy at a given external magnetic field was $\hbar\omega_c = 0.172$ meV. Furthermore, the electron-photon coupling strength was fixed at $g_\gamma = 0.1$ meV. In order to obtain the thermoelectric and heat currents in the system, we considered the chemical potential of the leads to be equal $\mu_L = \mu_R$, and the temperature of the leads were changed.

3.1. The Quantum Wire without Photon Field

We first considered the quantum wire without coupling to the photon field in the cavity. Figure 2 shows the energy spectrum of the leads (a) and the quantum wire (b) in the case of no photon field.

In Figure 2a, the single-electron (SE) energy spectrum in the leads (green) versus wave-number q scaled by the effective magnetic length a_w^{-1} is plotted. The first sub-band, $ny = 0$, participate in the propagating modes, while higher sub-bands contribute to the evanescent modes. In Figure 2b, the many-electron (ME) energy spectrum of the quantum wire is demonstrated in which the Coulomb interaction is taken into account, while no electron-photon coupling has been defined. The lowest one-electron states of the quantum wire are presented here such as the ground-state (G) with energy value $E_G = 1.25$ meV, the first- (FE) with $E_{FE} = 1.98$ meV, the second- (SE) with $E_{SE} = 3.23$ meV, and the third-excited state (TE) with $E_{TE} = 3.26$ meV, respectively. The two-electron states are located

at relatively higher energies due to the electron-electron repulsion effect in the quantum wire (not shown). The electron states of the quantum wire were almost doubly degenerate due to the small Zeeman energy. In addition, the SE and the TE states were nearly degenerate due to the geometry of the quantum wire.
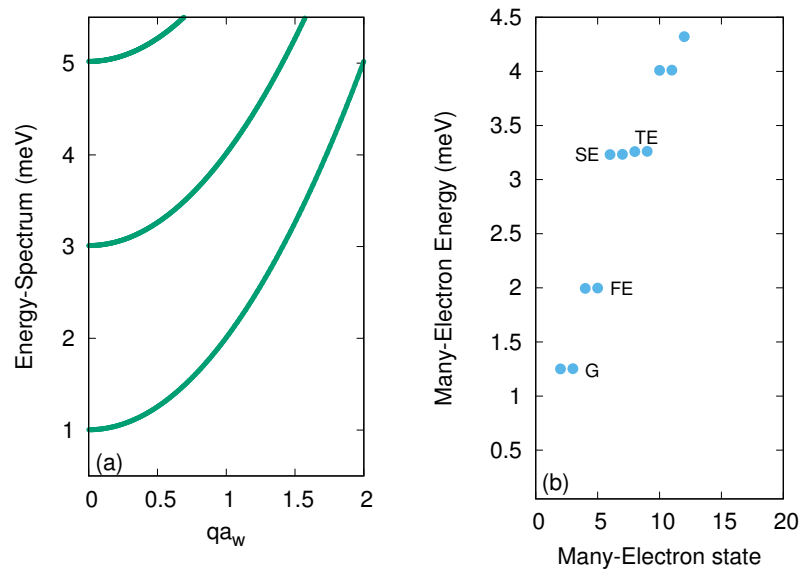

Figure 2. (Color online) Energy spectra in the case of no photon field. (**a**) Energy-spectrum of the single-electron sub-bands of the leads (green) as a function of wave number q is plotted. (**b**) Many-electron energy spectrum of the quantum wire as a function of the many-electron state is presented. The many-electron state of the quantum wire is almost doubly-degenerate due to the small Zeeman energy. G, FE, SE, and TE indicate the one-electron ground-state, first-excited state, second-excited state, and third-excited state, respectively. The magnetic field is $B = 0.1$ T, and $\hbar\Omega_0 = 2.0$ meV.

To calculate the thermal properties of the system, we present Figure 3, which shows the heat current (a), thermoelectric current (b), and occupation (c) of the quantum wire without the photon field where the temperatures of the leads are $T_L = T_h = 1.16$ and $T_R = T_c = 0.58$ K.

The vertical golden lines are the resonance places of the chemical potential of leads with G (left line) and FE (right line). The heat current was almost zero at both resonance energy states, G and EF, and had a positive value between the states (see Figure 3a). This can be understood by the heat current equation presented in Equation (8). If the chemical potential of the leads is located below the energy state, $\mu < E_i$, the first term of the heat current equation, $(i|\hat{\rho}_S^{h,c}|j)$, and the second term, $E_i - \mu$, are both positive. Therefore, the heat current is always positive. Above the resonant state, $\mu > E_i$, the first and the second terms are both negative, resulting in the positive value of the heat current.
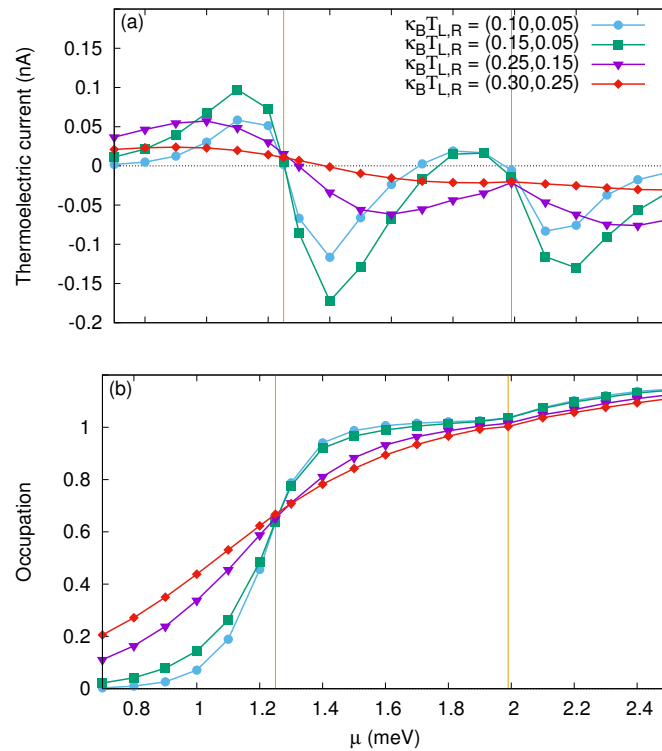
In Figure 3b, the thermoelectric current is presented in the case of no photon field. The properties of thermoelectric current can be explained by the Fermi functions of the external leads or the occupation of the system.

The thermoelectric current is zero when the occupation (Fermi functions of the leads) is equal to half filling (0.5) or integer filling zero or one [38,39]. Therefore, the thermoelectric current was almost zero at $\mu = 1.25$ meV, corresponding to the half filling occupation of the G state shown in Figure 3c. Furthermore, the thermoelectric current was again zero at $\mu = 0.7$ and $\mu = 1.7$ meV corresponding to the occupation of zero and one [40].
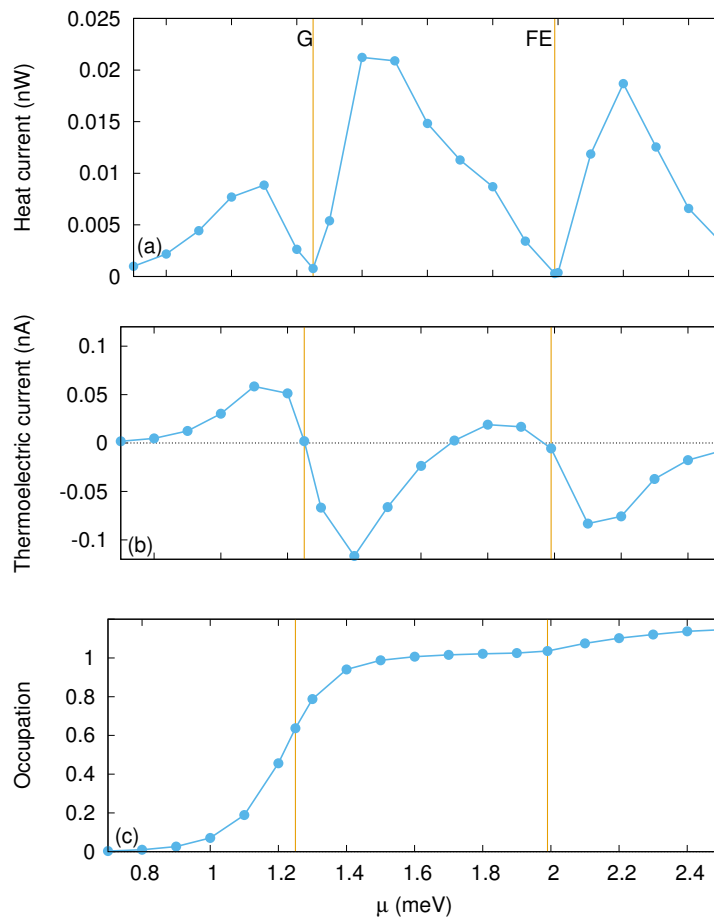
Figure 3. (Color online) Heat current (**a**), thermoelectric current (**b**), and occupation (**c**) as functions of the chemical potential $\mu = \mu_L = \mu_R$ are plotted at time $t = 220$ ps. in the case of no photon field. The temperatures of the leads are $T_h = 1.16$ and $T_c = 0.58$ K, implying thermal energy of 0.1 and 0.05 meV, respectively. The golden vertical lines show the resonance condition for the ground state at $\mu = 1.25$ meV and the first-excited state at $\mu = 1.98$ meV, respectively. The magnetic field is $B = 0.1$ T, and $\hbar\Omega_0 = 2.0$ meV.

If the temperature of the leads is increased to a higher value, the thermoelectric current may lose its oscillatory behavior around the resonance states. Figure 4 shows the thermoelectric current (a) and the occupation (b) for different temperatures of the leads. For example, if the temperature of the left lead increased to $\simeq 1.74$ K and the temperature of the right lead was kept constant at 0.58 K, which corresponds to the thermal energy 0.15 and 0.05 meV (green squares), respectively, the thermoelectric current was enhanced, and it was oscillating around both G and FE states. The positivity and negativity behavior of the thermoelectric current can still be seen. If the temperatures of both leads was increased (purple triangles and red diamonds), the thermoelectric current and the occupation were smeared out due to the thermal smearing effect. As a result, nearly a plateau in the thermoelectric current was observed at thermal energy $(0.30, 0.25)$ (red diamonds). The reason is that the thermal broadening of the leads is higher than the energy spacing between G and FE here. Therefore, the oscillatory behavior of thermoelectric current around these states vanished.

Figure 4. (Color online) Thermoelectric current (**a**), and occupation (**b**) as functions of the chemical potential $\mu = \mu_L = \mu_R$ plotted at time $t = 220$ ps. The thermal energy is $\kappa_B T_{h,c} = (0.1, 0.05)$ (blue circles), $(0.15, 0.05)$ (green squares) $(0.25, 0.15)$ (purple triangles), and $(0.30, 0.25)$ (red diamonds). The golden vertical lines show the resonance condition for the ground state at $\mu = 1.25$ meV and the first-excited state at $\mu = 1.98$ meV, respectively. The magnetic field is $B = 0.1$ T, and $\hbar\Omega_0 = 2.0$ meV.

3.2. The Quantum Wire with Photon Field

We now assume the quantum wire is coupled to a photon field with *x*-polarization and initially one photon in the cavity $N_\gamma = 1$. A single photon was used to control thermal transport in the quantum wire. The temperature of the leads was fixed at $T_L = T_h = 1.16$ and $T_R = T_c = 0.58$ K, implying thermal energy of 0.1 and 0.05 meV, respectively. We assumed two resonant regimes with the electron-photon coupling strength $g_\gamma = 0.1$ meV. First, it was considered that the photon energy was approximately equal to the energy spacing between G and FE, $\hbar\omega_\gamma \simeq E_{FE} - E_G = 0.74$ meV. The energy spectrum of the lowest states in this case is shown in Figure 5a. Secondly, the photon energy was approximately equal to the energy spacing between G and SE, $\hbar\omega_\gamma \simeq E_{SE} - E_G = 1.98$ meV, as is presented in Figure 5b. In both cases, the quantum wire was in resonance with the photon cavity.

In the presence of the cavity, when the photon energy was $\hbar\omega_\gamma = 0.74$ meV (see Figure 5a), photon replica states were formed in addition to the original states of the quantum wire. For instance, the one-photon replica ($G_{1\gamma}$) of the ground-state near the FE was found, indicating the resonance of the quantum wire with the cavity. In addition, the two-photon replica ($G2\gamma$) of the ground-state and the one-photon replica ($FE_{1\gamma}$) of the first-excited state were seen around the energy range of 2.6–2.9 meV. In the second resonance regime, when the photon energy was $\hbar\omega_\gamma = 1.98$ meV (see Figure 5b), the one-photon replica ($G_{1\gamma}$) of the ground-state near the SE was formed. These photon replica states play an important role in the electron transport in the system.

To see the effects of the photon field on the transport properties of the system, the heat current (a) and the thermoelectric current (b) are demonstrated in Figure 6 for the quantum wire without (w/o ph) (blue circles) and with the photon field, with the photon energy of $\hbar\omega_\gamma = 0.74$ (green squares) and 1.98 meV (red triangles).
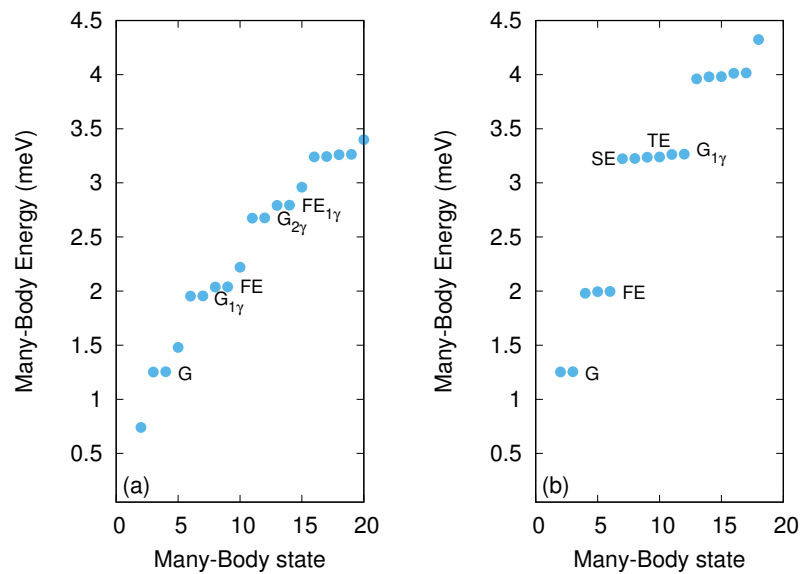
Figure 5. (Color online) Many-body energy spectrum of the quantum wire coupled to the photon field as a function of the many-body state. The photon energy is assumed to be $\hbar\omega_\gamma = 0.74$ meV (**a**) and $\hbar\omega_\gamma = 1.98$ meV (**b**). The many-electron state of the quantum wire is almost doubly-degenerate due to the small Zeeman energy. G, FE, SE, and TE indicate the one-electron ground-state, first-excited state, second-excited state, and third-excited state, respectively. Comparing to Figure 2b, extra states are formed, which are $G_{1\gamma}$ and $FE_{1\gamma}$, referring to the one-photon replica of the ground-state and the first-excited, state while $G_{2\gamma}$ indicates the two-photon replica of the ground-state. The magnetic field is $B = 0.1$ T, and $\hbar\Omega_0 = 2.0$ meV.
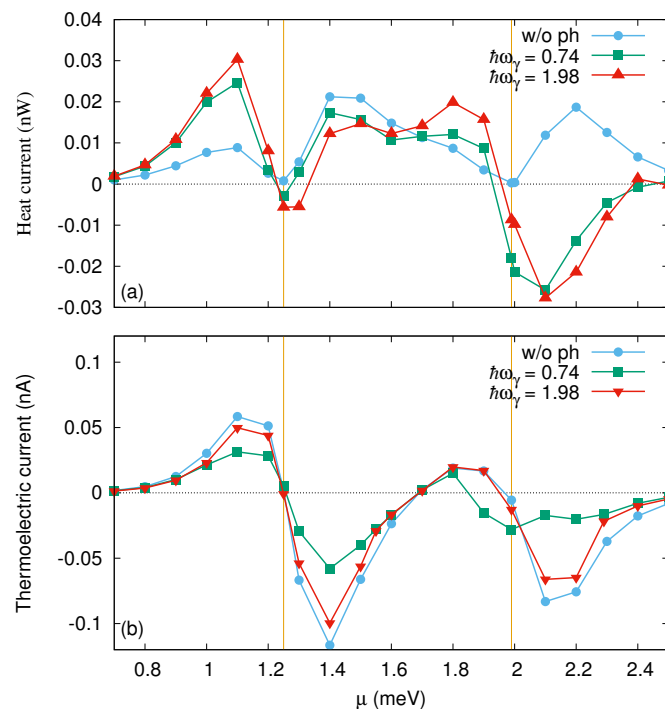
Figure 6. (Color online) Heat current (**a**) and thermoelectric current (**b**) as functions of chemical potential of the leads plotted at time $t = 220$ ps for the system without (w/o) photon field (ph) (blue circles) and with the photon field with photon energy of 0.74 (green squares) and 1.98 meV (red triangles). The temperatures of the leads are $T_h = 1.16$ and $T_c = 0.58$ K, implying thermal energy of 0.05 meV and 0.1, respectively. The magnetic field is $B = 0.1$ T, and $\hbar\Omega_0 = 2.0$ meV.

In the presence of the cavity, the photon replica states $G_{1\gamma}$ and $FE_{1\gamma}$ together with G and FE were actively participating in the transport. We divided our results into three regions of the chemical potential with respect to the energy states of the quantum wire which were the following regions, $\mu < E_G$, $E_G < \mu < E_{FE}$, and $\mu > E_{FE}$.

We start with the first range when the chemical potential of the leads is less than the ground-state energy $\mu < E_G = 1.25$ meV. In this case, both G and $G_{1\gamma}$ contributed to the electron transport. One may want to explain the characteristics of heat current from the heat current equation and see both terms of Equation (8) give positive values. Especially, the first term $(i|\hat{\rho}_S^{h,c}|j)$ was increased to almost twice of its value in the absence of the cavity due to the participation of both G and $G_{1\gamma}$. The heat current was thus enhanced for both photon energies, 0.74 (green squares) and 1.98 meV (red triangles). In the same range, $\mu < 1.25$ meV, the thermoelectric current was slightly suppressed, which was due to the radiative transition of $G_{1\gamma}$ in the electron transport [34].

In the second range, when $E_G = 1.25$ meV $< \mu < E_{FE} = 1.98$ meV, the heat current was slightly suppressed since the $G_{1\gamma}$ was located above the chemical potential, while G was below the chemical potential in this range. Therefore, the second term of Equation (8), $(E_i - \mu\hat{N}_e)$, for the G became negative, leading to a decrease in the heat current for both photon energies. Furthermore, the thermoelectric current was again suppressed. The mechanism of electron transport via G and $G_{1\gamma}$ is different here. The electron went from the cold lead to the hot lead via G because it was located below the chemical potential. However, the electron transport via $G_{1\gamma}$ was totally opposite, going from the hot lead to the cold lead since it was located above μ. As a result, the thermoelectric current decreased.

In the last range, when $\mu > E_{FE} = 1.98$ meV, FE and $FE_{1\gamma}$ participated in the electron transport and had the same mechanism of transport as G and $G_{1\gamma}$. $G_{1\gamma}$ was still active in the transport in this range. Therefore, the negativity in the heat current was observed.

The above explanations regarding the contribution of the photon replica states to the transport may not be applicable at a higher thermal energy. Figure 7 shows the thermoelectric current versus the thermal energy for the system without (w/o) (blue circles) and with the photon field at the photon energy $\hbar\omega_\gamma = 0.74$ (green squares) and 1.98 meV (red triangles). We here fixed the chemical potential of the leads at $\mu = 1.1$ meV located just below G. Furthermore, the temperature of the right lead was fixed at $T_c = 0.58$ K, and the temperature of the left lead was tuned.
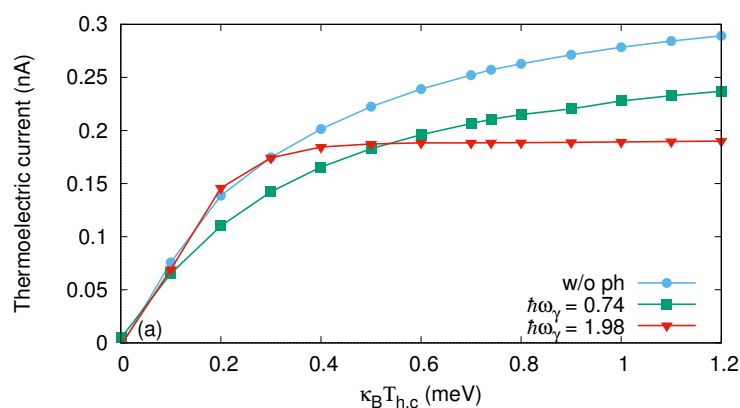
Figure 7. (Color online) Thermoelectric current as functions of thermal energy $\kappa_B T_{h,c} = \kappa_B(T_h - T_c)$ plotted at time $t = 220$ ps for the system without (w/o) the photon field (blue circles) and with the photon field with photon energy 0.75 (green squares) and 1.98 meV (red triangles). The chemical potential is fixed at $\mu = \mu_L = \mu_R = 1.1$ meV. The temperature of the right lead is fixed at $T_R = T_c = 0.58$ K, implying thermal energy of 0.05 meV, and a varying the temperature of the left lead ($T_L = T_h$). The magnetic field is $B = 0.1$ T, and $\hbar\Omega_0 = 2.0$ meV.

It can be clearly seen that the thermoelectric current was further suppressed for the photon energy $\hbar\omega_\gamma = 1.98$ meV at high thermal energy, especially above 0.6 meV. The reason here is that the $G_{1\gamma}$

became further active in the electron transport due to thermal smearing. As a result, the thermoelectric current was further suppressed.

4. Conclusions

To conclude, we have analyzed thermoelectric effects in a quantum wire attached to two electronic reservoirs of different temperatures. The two-dimensional quantum wire was coupled to a quantized photon field in a 3D-cavity, leading to the electron–photon interaction. A fully-quantized photon field with a single photon was utilized to control thermal transport in a short quantum wire. It should be mentioned that this is a novel technique to control thermal transport in nanodevices. We have studied not only the thermally-induced charge current between the two reservoirs, but also the thermally-induced heat current. Numerical results on the thermal transport show that the heat current and thermoelectric current can be controlled by a single photon. We can tune the cavity parameters, such as photon energy, in such a way that the thermal transport can be enhanced. The enhancement of thermal transport is due to the participation of the photon replica states formed in the presence of the cavity in the transport. As a consequence, our method can be seen as a new technique to control heat and thermoelectric currents in nanoscale systems using a single photon source.

Abbreviations

The following abbreviations are used in this manuscript:

ZT	Figure of merit
G	Ground-state energy
$G_{1\gamma}$	One-photon replica of the ground-state
$G_{2\gamma}$	Two-photon replica of the ground-state
FE	First-excited state energy
$FE_{1\gamma}$	One-photon replica of the first-excited state energy
SE	Second-excited state energy
TE	Third-excited state energy

References

1. Yoon, H.S.; Lee, J.Y.; Kim, H.S.; Kim, M.S.; Kim, E.S.; Shin, Y.J.; Chu, W.S.; Ahn, S.H. A comparison of energy consumption in bulk forming, subtractive, and additive processes: Review and case study. *Int. J. Precis. Eng. Manuf. Green Technol.* **2014**, *1*, 261–279. [CrossRef]
2. Pérez-Lombard, L.; Ortiz, J.; Pout, C. A review on buildings energy consumption information. *Energy Build.* **2008**, *40*, 394–398. [CrossRef]
3. Canovas-Carrasco, S.; Garcia-Sanchez, A.J.; Garcia-Haro, J. A nanoscale communication network scheme and energy model for a human hand scenario. *Nano Commun. Netw.* **2018**, *15*, 17–27. [CrossRef]
4. Aricò, A.S.; Bruce, P.; Scrosati, B.; Tarascon, J.M.; van Schalkwijk, W. Nanostructured materials for advanced energy conversion and storage devices. *Nat. Mater.* **2005**, *4*, 366–377. [CrossRef] [PubMed]
5. Pop, E. Energy dissipation and transport in nanoscale devices. *Nano Res.* **2010**, *3*, 147–169. [CrossRef]

6. Ren, J.; Zhu, J.X.; Gubernatis, J.E.; Wang, C.; Li, B. Thermoelectric transport with electron-phonon coupling and electron-electron interaction in molecular junctions. *Phys. Rev. B* **2012**, *85*, 155443. [CrossRef]

7. Talbo, V.; Saint-Martin, J.; Retailleau, S.; Dollfus, P. Non-linear effects and thermoelectric efficiency of quantum dot-based single-electron transistors. *Sci. Rep.* **2017**, *7*, 14783. [CrossRef]

8. Snyder, G.J.; Snyder, A.H. Figure of merit ZT of a thermoelectric device defined from materials properties. *Energy Environ. Sci.* **2017**, *10*, 2280–2283. [CrossRef]

9. Szczech, J.R.; Higgins, J.M.; Jin, S. Enhancement of the thermoelectric properties in nanoscale and nanostructured materials. *J. Mater. Chem.* **2011**, *21*, 4037–4055. [CrossRef]

10. Majumdar, A. Thermoelectricity in Semiconductor Nanostructures. *Science* **2004**, *303*, 777–778. [CrossRef]

11. Heremans, J.P.; Dresselhaus, M.S.; Bell, L.E.; Morelli, D.T. When thermoelectrics reached the nanoscale. *Nat. Nanotechnol.* **2013**, *8*, 471–473. [CrossRef] [PubMed]

12. Alam, H.; Ramakrishna, S. A review on the enhancement of figure of merit from bulk to nano-thermoelectric materials. *Nano Energy* **2013**, *2*, 190–212. [CrossRef]

13. Harman, T.C.; Taylor, P.J.; Spears, D.L.; Walsh, M.P. Thermoelectric quantum-dot superlattices with high ZT. *J. Electron. Mater.* **2000**, *29*, L1–L2. [CrossRef]

14. Sothmann, B.; Sánchez, R.; Jordan, A.N. Thermoelectric energy harvesting with quantum dots. *Nanotechnology* **2015**, *26*, 032001. [CrossRef] [PubMed]

15. Trocha, P.; Barnaś, J. Large enhancement of thermoelectric effects in a double quantum dot system due to interference and Coulomb correlation phenomena. *Phys. Rev. B* **2012**, *85*, 085408. [CrossRef]

16. Wierzbicki, M.; Swirkowicz, R. Influence of interference effects on thermoelectric properties of double quantum dots. *Phys. Rev. B* **2011**, *84*, 075410. [CrossRef]

17. Wang, Q.; Xie, H.; Nie, Y.H.; Ren, W. Enhancement of thermoelectric efficiency in triple quantum dots by the Dicke effect. *Phys. Rev. B* **2013**, *87*, 075102. [CrossRef]

18. Hicks, L.D.; Dresselhaus, M.S. Effect of quantum-well structures on the thermoelectric figure of merit. *Phys. Rev. B* **1993**, *47*, 12727–12731. [CrossRef]

19. Liu, J.; Sun, Q.F.; Xie, X.C. Enhancement of the thermoelectric figure of merit in a quantum dot due to the Coulomb blockade effect. *Phys. Rev. B* **2010**, *81*, 245323. [CrossRef]

20. Kolenda, S.; Wolf, M.J.; Beckmann, D. Observation of Thermoelectric Currents in High-Field Superconductor-Ferromagnet Tunnel Junctions. *Phys. Rev. Lett.* **2016**, *116*, 097001. [CrossRef]

21. Bathen, M.E.; Linder, J. Spin Seebeck effect and thermoelectric phenomena in superconducting hybrids with magnetic textures or spin-orbit coupling. *Sci. Rep.* **2017**, *7*, 41409. [CrossRef] [PubMed]

22. Karwacki, L.; Barnaś, J. Thermoelectric properties of a quantum dot coupled to magnetic leads by Rashba spin-orbit interaction. *Phys. Rev. B* **2018**, *98*, 075413. [CrossRef]

23. Abdullah, N.R.; Arnold, T.; Tang, C.S.; Manolescu, A.; Gudmundsson, V. Photon-induced tunability of the thermospin current in a Rashba ring. *J. Phys. Condens. Matter* **2018**, *30*, 145303. [CrossRef]

24. Abdullah, N.R.; Tang, C.S.; Manolescu, A.; Gudmundsson, V. Spin-dependent heat and thermoelectric currents in a Rashba ring coupled to a photon cavity. *Phys. E Low-Dimens. Syst. Nanostruct.* **2017**, *95*, 102–107. [CrossRef]

25. Abdullah, N.R.; Tang, C.S.; Manolescu, A.; Gudmundsson, V. Effects of photon field on heat transport through a quantum wire attached to leads. *Phys. Lett. A* **2018**, *382*, 199–204. [CrossRef]

26. Abdullah, N.R. Optical control of spin-dependent thermal transport in a quantum ring. *Phys. Lett. A* **2018**, *382*, 1432–1436. [CrossRef]

27. Ojanen, T.; Jauho, A.P. Mesoscopic Photon Heat Transistor. *Phys. Rev. Lett.* **2008**, *100*, 155902. [CrossRef]

28. Joulain, K.; Drevillon, J.; Ezzahri, Y.; Ordonez-Miranda, J. Quantum Thermal Transistor. *Phys. Rev. Lett.* **2016**, *116*, 200601. [CrossRef] [PubMed]

29. Meschke, M.; Guichard, W.; Pekola, J.P. Single-mode heat conduction by photons. *Nature* **2006**, *444*, 187–190. [CrossRef] [PubMed]

30. Chi, F.; Dubi, Y. Microwave-mediated heat transport in a quantum dot attached to leads. *J. Phys. Condens. Matter* **2012**, *24*, 145301. [CrossRef]

31. Abdullah, N.R. Magnetically and Photonically Tunable Double Waveguide Inverter. *IEEE J. Quantum Electron.* **2016**, *52*, 1–6. [CrossRef]

32. Abdullah, N.R.; Fatah, A.H.; Fatah, J.M.A. Effects of magnetic field on photon-induced quantum transport in a single dot-cavity system. *Chin. Phys. B* **2016**, *25*, 114206. [CrossRef]

33. Abdullah, N.R.; Tang, C.S.; Manolescu, A.; Gudmundsson, V. Coherent transient transport of interacting electrons through a quantum waveguide switch. *J. Phys. Condens. Matter* **2015**, *27*, 015301. [CrossRef] [PubMed]

34. Gudmundsson, V.; Jonsson, T.H.; Bernodusson, M.L.; Abdullah, N.R.; Sitek, A.; Goan, H.S.; Tang, C.S.; Manolescu, A. Regimes of radiative and nonradiative transitions in transport through an electronic system in a photon cavity reaching a steady state. *Annalen der Physik* **2017**, *529*, 1600177. [CrossRef]

35. Abdullah, N.R.; Tang, C.S.; Manolescu, A.; Gudmundsson, V. Delocalization of electrons by cavity photons in transport through a quantum dot molecule. *Physica E* **2014**, *64*, 254–262. [CrossRef]

36. Abdullah, N.R.; Tang, C.S.; Manolescu, A.; Gudmundsson, V. Optical switching of electron transport in a waveguide-QED system. *Phys. E Low-Dimens. Syst. Nanostruct.* **2016**, *84*, 280–284. [CrossRef]

37. Abdullah, N.R.; Tang, C.S.; Manolescu, A.; Gudmundsson, V. Competition of static magnetic and dynamic photon forces in electronic transport through a quantum dot. *J. Phys. Condens. Matter* **2016**, *28*, 375301. [CrossRef]

38. Tagani, M.B.; Soleimani, H.R. Photon–phonon -assisted thermoelectric effects in the molecular devices. *Phys. E Low-Dimens. Syst. Nanostruct.* **2013**, *48*, 36–41. [CrossRef]

39. Golsanamlou, Z.; Vishkayi, S.I.; Tagani, M.B.; Soleimani, H.R. Thermoelectric properties of metal/molecule/metal junction for different lengths of polythiophene. *Chem. Phys. Lett.* **2014**, *594*, 51–57. [CrossRef]

40. Abdullah, N.R.; Tang, C.S.; Manolescu, A.; Gudmundsson, V. Cavity-Photon Controlled Thermoelectric Transport through a Quantum Wire. *ACS Photonics* **2016**, *3*, 249–254. [CrossRef]